



The Effect of Cooling Rate on Solidification Characteristics and Grain Structure of Al-9Si Cast Alloy

Ma Xian Hui¹, Nur Azhani Abd Razak^{1,*}, Asnul Hadi Ahmad^{1,2}, Juliawati Alias^{1,2}, Nasrul Azuan Alang¹

¹ Faculty of Mechanical and Automotive Engineering Technology, Universiti Malaysia Pahang, 26600 Pekan, Pahang, Malaysia

² Centre for Automotive Engineering, Universiti Malaysia Pahang, 26600 Pekan, Pahang Darul Makmur, Malaysia

ARTICLE INFO

Article history:

Received 28 June 2024

Received in revised form 22 September 2024

Accepted 30 September 2024

Available online 20 October 2024

Keywords:

Aluminium alloy; semisolid metal processing; thermal analysis; cooling rate; microstructure formation

ABSTRACT

A thermal analysis study is essential before the semisolid metal processing of a particular alloy. The surrounding environment, especially the cooling rate is also an important factor. This study investigated the influence of different cooling rates on the solidification characteristics and microstructure evolution of the Al-9Si cast alloy. Four cooling mediums were designed, and their cooling rates are 0.16 °C/s, 1.0 °C/s, 1.3 °C/s, and 1.9 °C/s, respectively. The results show that the primary dendrite size of the Al-9Si alloy was reduced from 162.61 μm to 86.86 μm as the cooling rate increased from 0.16 °C/s to 1.9 °C/s. Significant grain refinement was observed, however, the external cooling has a negligible impact on solid fraction. The optimal temperature range of the Al-9Si cast alloy for the semisolid metal processing at a solid fraction of 0.5 to 0.7 is between 554 °C and 563 °C. With these thermal profiles provided, the relationship between the solid fraction and the solidification time could be expressed using the polynomial equation, which is also useful for point prediction in the subsequent semisolid metal processing.

1. Introduction

Direct thermal method (DTM) is a thixotropic feedstock production technique developed by researchers at University College Dublin [1]. It is a simple and cost-saving treatment to produce billets with nearly globular microstructure for the subsequent thixoforming. Thixoforming is one of the semisolid metal (SSM) processing technologies which offer several advantages over conventional high-pressure die casting (HPDC), such as products with fine and spherical microstructure formation, improved mechanical properties, minimised material and energy consumption, lower thermal shock enabling die life prolonged, as well as reduced processing cost on thixoformed parts owing to its improved usage of feedstock materials [2-6].

In DTM, the process involves pouring a low superheat liquid alloy into a low thermal mass cylindrical mould with high thermal conductivity. The alloy is treated in a pseudo-isothermal holding until it reaches a semisolid state with desired fraction solid. It is then followed by a water-quenching

* Corresponding author.

E-mail address: azhani@ump.edu.my

<https://doi.org/10.37934/arfmts.122.2.8393>

at room temperature to produce the thixotropic feedstock billets needed in the later process for thixoforming. It is believed that the microstructure in the semisolid state consists of solid-phase spheroids enclosed in a liquid phase, allowing laminar cavity fill, which could contribute to reduced gas entrapment [7,8]. Therefore, the determination of the most suitable processing parameters, especially the pouring temperature and the holding time, should be carefully considered, as it would affect the resulting microstructure formation.

It is important to note that the processing parameters are directly associated to the solidification characteristics of the alloy, for instance, the liquidus (T_L), eutectic (T_E), solidus (T_S) and dendrite coherency (T_{DCP}) temperatures. Solidification of an alloy begins at the liquidus point and ends at the solidus point. Besides, the dendrite coherency temperature marks the point of impingement of the dendrites where the mechanical strength development begins [9]. The thermal profile of a solidifying alloy is crucial in the DTM experiment which could be used to display the solid fraction curve corresponding to temperature along the solidification path, allowing users to ease the process parameter determination. It is noteworthy that the solid fraction significantly impacts the viscosity of the mush [10]. Kirkwood *et al.*, [11] proposed that an effective amount of fraction solid for thixoforming should be between 0.5 and 0.6. It is due to the billet becoming too soft to support its own weight for fraction solid below 0.5, whereas if it is above 0.6, the billet will become too stiff to flow and will not fill in the die for fraction solid. Other related studies also endorsed that the appropriate solid fraction range should be between 0.5 to 0.7 as by limiting the liquid fraction in semisolid, both the solidification range and the shrinkage can be controlled [12]. Nevertheless, some considerations should be considered; for example, the more complex geometry and larger parts would require higher liquid fractions. In short, the optimal solid fraction at which desired properties of the material are attained for SSM processing hinges on the material and process selection.

Hence, a thermal analysis study is certainly required before executing the DTM experiment. However, there is less literature to include the thermal analysis methodology before the determination of the optimal processing parameter in DTM. Moreover, it was reported that the addition of external cooling agent surrounding the copper mould in the DTM process significantly improves the microstructure refinement by 36.4 % [13]. It implies that the presence of a cooling agent could result in a better formation of the desired microstructure. Therefore, the magnitude or the intensity of the cooling rate becomes the topic of interest in the present study. The study aims to investigate the thermal properties and the microstructure evolution of Al-9Si cast alloy upon the alteration of the cooling rate to determine the suitable processing parameter in DTM.

2. Methodology

The as-received sample for the studied material was examined through optical emission spectroscopy to obtain the average composition reading, as shown in Table 1.

Table 1
Chemical composition of the as-received sample

Material	Composition, wt%								
	Al	Si	Zn	Cu	Fe	Ni	Mn	Mg	Others
As-received sample	81.5	9.76	1.48	1.16	0.69	0.54	0.31	0.23	Rem.

About 350 g of the specimen was prepared inside a graphite crucible with a dimension of 43 mm in diameter and 110 mm in depth, for each experimental run. The crucible was then heated up to 830 °C by an induction furnace, and the heating process was held for about 5 minutes for homogenisation of the melt. The experiment was designed with four different cooling mediums.

Their respective specimens were termed specimens A, B, C, and D from lowest to highest cooling rate, as summarised in Table 2.

Table 2
 Specimens were solidified in different cooling medium

Specimen	Cooling Medium
A	Cooled inside a kaowool chamber
B	Crucible's top and bottom are covered with kaowool sheets while its body open to the atmosphere
C	Natural ambient cooling
D	Compressed airflow

During the experiments, two K-type thermocouples were inserted inside the crucible to obtain the cooling curves at wall and centre. They were immersed about 90 mm in depth, and 20 mm apart from one another. DasyLab and NI 9219 were used for data logging. Figure 1 illustrates the thermal analysis experimental setup for a slow cooling condition.

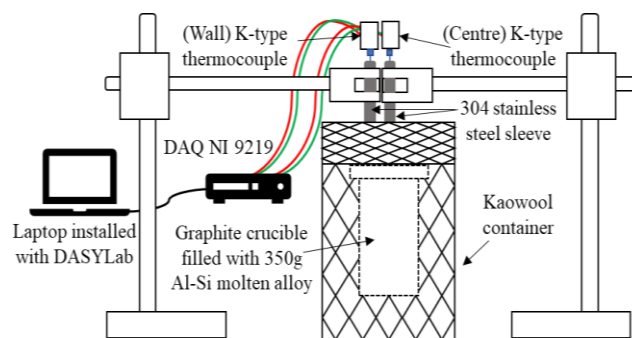


Fig. 1. Thermal analysis experimental setup for a slow cooling condition. A kaowool blanket fully enclosed the graphite crucible containing specimen A for the best thermal insulation effect

The cooling rate for each experiment was calculated by taking the temperature difference between the initial reading (680 °C) and the final reading (at which the temperature point was located 50 °C above the liquidus point of the specimen) and then dividing it by the time taken in seconds. The unit for cooling rate would be °C/s, and its equation is shown as follows

$$\text{Cooling rate} = \frac{T_o - T_{L+50^\circ\text{C}}}{t_o - t_{L+50^\circ\text{C}}} \quad (1)$$

Data smoothing and plotting of the cooling curve, cooling rate curve (commonly called first derivative curve), temperature difference curve, zero curves (or baseline), and fraction solid curve were created with the aid of OriginPro 2019b as a graphical representation tool. In theory, the impingement that occurred in the coherent dendrite network increases the thermal conductivity of the liquid and solid mixture, resulting in a reduction of the temperature difference, ΔT , between the wall and the centre of the crucible [14]. Therefore, the dendrite coherency point could be found in the temperature difference curve by detecting the first minimal point within the solidification temperature range [15]. Based on the solid fraction curve, the amount of heat that evolved from a solidifying specimen was calculated by measuring the area between the first derivative curve and the baseline [14].

While in the present study of metallography concerning different cooling rates, all specimens were cut into a section where the thermocouple tips were previously located. Each sectioned part was about 15 mm thick and further sectioned into quadrant-like pieces. Three samples for each specimen were chosen for the hot-mounting process. Next, these samples were mounted on the ground surface with 800-, 1200-, and 2400-grit size silicon carbide papers and continued with surface polishing by using 6-, 3-, and 1-micron diamond suspension with a different polishing cloth. The final polishing stage was done by 0.05-micron colloidal silica suspension. After that, the etching process was carried out on the polished samples by swabbing the samples' surfaces with Keller's reagent using a cotton bud. The swabbing process took around 5 seconds, and the samples' surfaces were immediately rinsed with water to remove etchant residue. After etching, the material's grain boundaries and interior structure were exposed and ready to be examined under the Olympus BX51M optical microscope while Motic Image Plus 3.0 ML software were used for microstructure characterisation. The image taken was set at 5x and 20x magnification. In the microstructure analysis, the primary grain structures of samples were inspected using ImageJ software to determine their diameter, circularity, and aspect ratio.

3. Results

3.1 Effects of Cooling Rate on Solidification Parameters

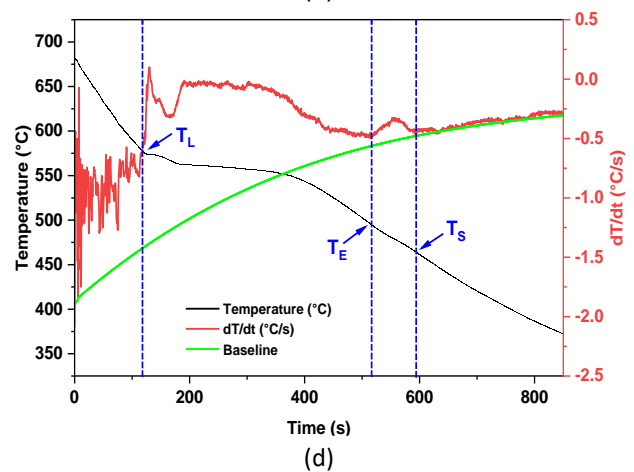
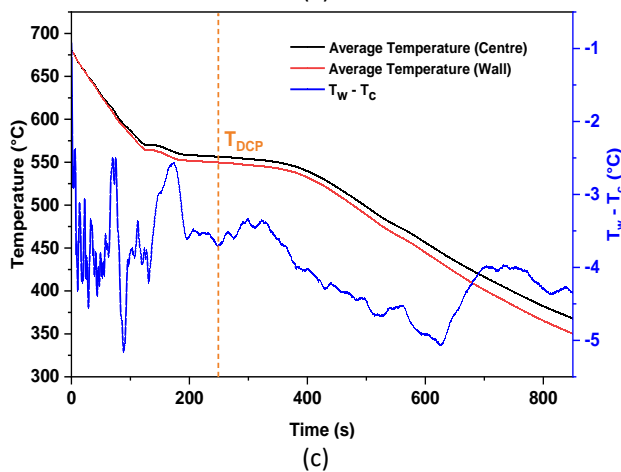
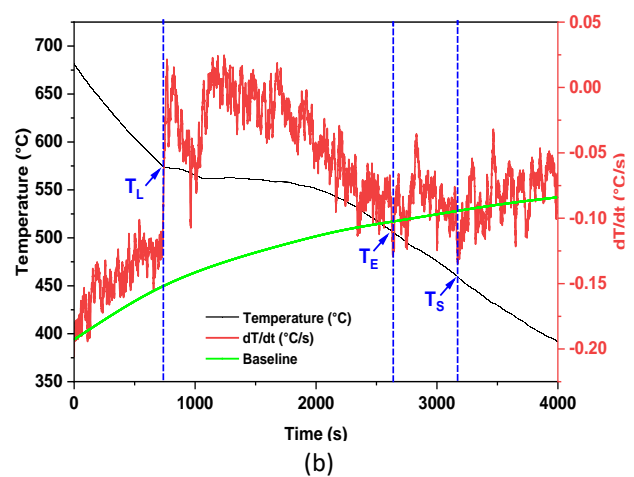
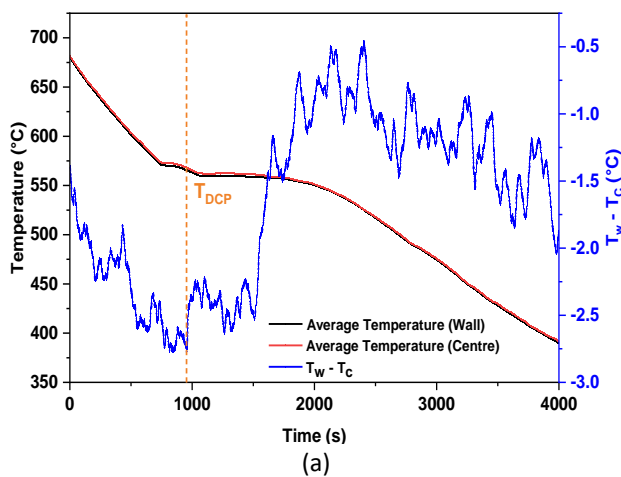
Upon the implementation of computer-aided cooling curve analysis, several important solidification parameters could be determined from the thermal profile, especially the liquidus, eutectic, solidus, and dendritic coherency points of the solidified material. The dendritic coherency point is a transition of alloy properties from liquid state to solid state, such as strength, thermal conductivity, and contraction [16]. The thermal profiles in Figure 2(a), Figure 2(c), Figure 2(e), and Figure 2(g) encompasses the cooling curve, cooling rate curve, and zero curves under different cooling rate conditions. The use of first derivatives eases the identification of the solidification characteristics on the cooling curve [16]. Also, the precipitation of a new phase that liberates latent heat will result in a sharp peak in the derivative curve. The derivative increases at the start of phase transformation and decreases at the end of phase transformation. For instance, in Figure 2(b), the intercepting point between the cooling curve and its first derivative curve denotes the liquidus temperature, T_L , where primary dendrites (α -Al) begin to solidify from the liquid. The change in the slope of the cooling curve at T_L results from the release of latent heat by the solidification of the alpha phase. The derivative curve at T_L surges rapidly due to the nucleation of α -Al and is succeeded by the growth and thickening of aluminium dendrites which results in the decline of the derivative curve. The eutectic reaction releases a large amount of latent heat, which leads to an increase in the derivative and is continued by the development of the secondary phase [16]. The solidus point, T_S corresponds to an inflection on the derivative curve denoting the end of the solidification. The dendritic coherency point was found at the minimal point of the temperature difference curve within the solidification range by employing the two-thermocouple method. The same working principle applies to the thermal profiles of the other cooling rate conditions in Figure 2(d), Figure 2(f), and Figure 2(h).

The baseline was generated to get the fraction solid to correspond to its solidifying temperature. The fraction solid curve was constructed by computing the area under the graph between the baseline and the first derivative curve within the solidification range. The aforementioned equation (1) was applied to measure the cooling rate at the slope of the cooling curve above the liquidus region. The cooling rates obtained in the present experimental work for different cooling conditions were 0.16 °C/s (slow cooling), 1.0 °C/s (intermediate cooling), 1.3 °C/s (normal cooling), and 1.9 °C/s

(fast cooling). Their thermal properties readings were recorded in Table 3. Based on the results shown in Table 3, each parameter` readings do not show a consistent trend and were fluctuated by the change of the cooling rate. The temperature variation of each parameter from the cooling rate of 0.16 °C/s to 1.9 °C/s: 6 °C in T_L ; 11 °C in both T_{DCP} and T_E ; 13 °C in T_S . However, the output value for the lowest cooling rate is much the same as for the highest cooling rate. It could be said that the external cooling has an insignificant impact on the solidification parameters.

Table 3
 Solidification parameters at four different cooling rate conditions

Specimen	Cooling Rate (°C/s)	T_L (°C)	T_{DCP} (°C)	T_E (°C)	T_S (°C)	ΔT (°C)	Δt (s)
A	0.16	574	568	506	459	115	2429
B	1.0	578	560	496	468	110	467
C	1.3	571	557	507	455	116	377
D	1.9	574	568	502	456	118	240



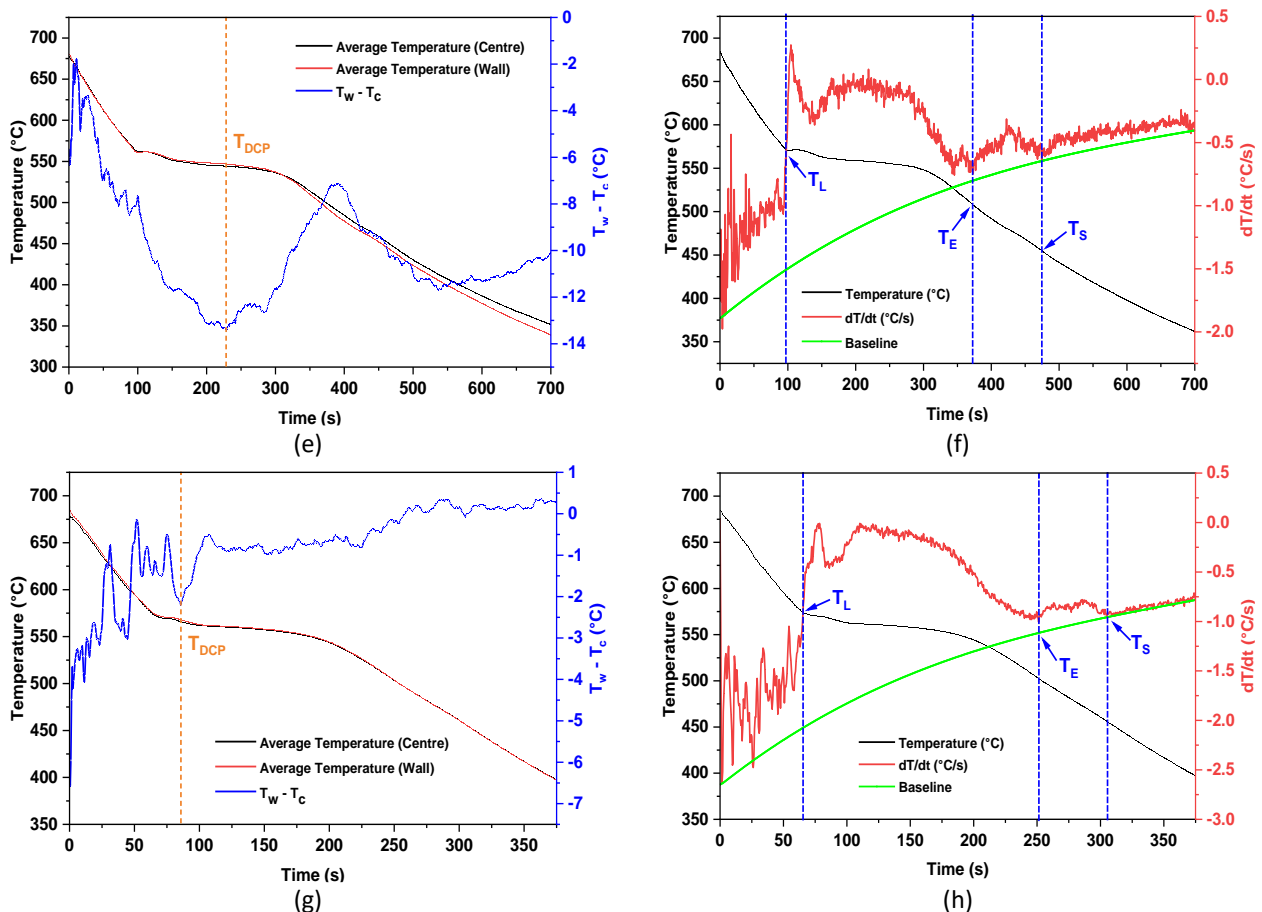


Fig. 2. Solidification characteristics and thermal profile of Al-9Si cast alloy which is subjected to cooling rate conditions of (a), (b) 0.16 °C/s, (c), (d) 1.0 °C/s, (e), (f) 1.3 °C/s, and (g), (h) 1.9 °C/s respectively

Figure 3(a) compares cooling curves with four different cooling rates. The solidification temperature ranges slightly varied from 110 °C to 118 °C. As for the solidification time, about 2429 seconds in slow cooling, 467 seconds in intermediate cooling, 377 seconds in normal cooling, and 240 seconds in fast cooling were taken to complete the solidification process. At a higher cooling rate, more heat is lost from the specimen, resulting in a steeper cooling curve slope and vice versa. Figure 3(b) illustrates solid fraction curves and their corresponding temperature at four different cooling rates. As mentioned in the literature, the optimal temperature range for SSM process control should be within 0.5 to 0.7 of solid volume fraction, and the material has a sufficient rigid form which could support its own weight for the thixoforming process; at the same time, the material flow rate and shrinkage could be well controlled and reduced. As displayed in Figure 3(b), the maximum and minimum temperature of solidifying material with several cooling rates at solid volume fraction, $f_s = 0.5$ are 563 °C and 558 °C with a temperature variation of 5 °C, whereas the maximum and minimum temperature at $f_s = 0.7$ is 558 °C and 554 °C with a temperature variation of 4 °C. The overall results found that the temperature variation at $f_s = 0.5$ and $f_s = 0.7$ is considerably small and that the fraction solid of material is not significantly affected by the change of cooling rate, which is in agreement with other finding [17].

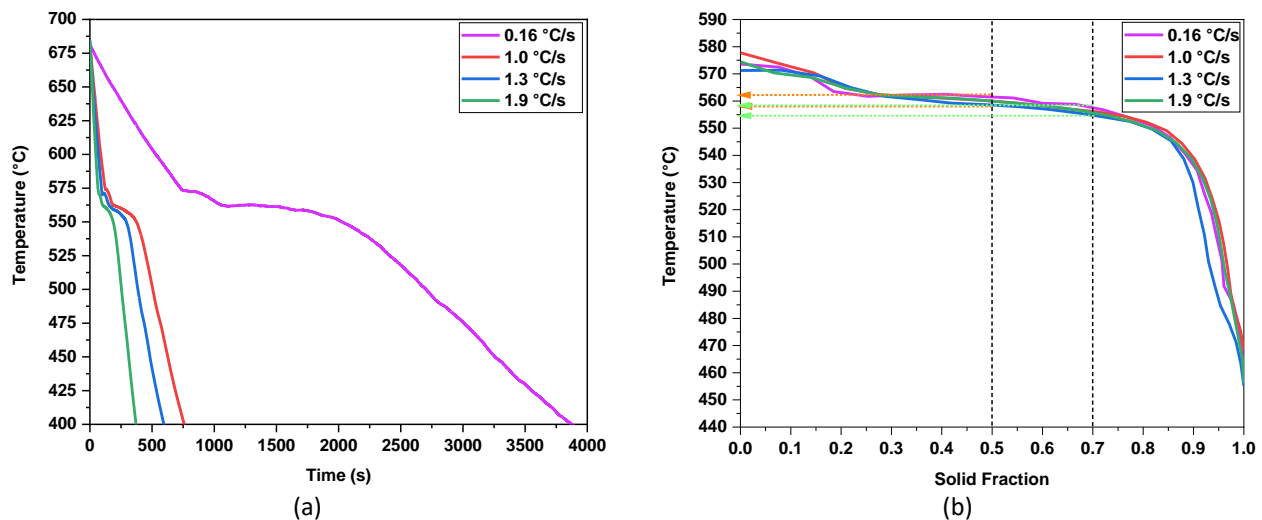


Fig. 3. (a) Cooling curves of four different cooling rate conditions. (b) Fraction solid curves and their corresponding temperatures at four different cooling rates

3.2 Effects of Cooling Rate on Primary Grain Structure

The impact of cooling rate on microstructure evolution was studied using qualitative and quantitative comparison methods. The microstructure images that are shown in Figure 4(a), Figure 4(c), Figure 4(e), and Figure 4(g) are the samples of cross-sectional areas at the crucible centre. In contrast, Figure 4(b), Figure 4(d), Figure 4(f) and Figure 4(h) are the samples of cross-sectional areas at the crucible wall. The samples subject to slow cooling in Figure 4(a) and Figure 4(b) were characterised by the presence of coarse primary phase grains and nonuniform eutectic distribution throughout the volume of a specimen. As the cooling rate increased from 0.16 °C/s to 1.9 °C/s, the size of primary phase crystals gradually reduced, and the eutectic became more dispersed and uniform. It is believed that individual coarse inclusions of binary eutectic Mg_2Si were observed (see red circle in figures) since the eutectic Mg_2Si was shaped as irregular Chinese characters, dendrites, or fishbones, as described in other studies [18]. These figures in elongated lamellar oval-shaped white area are the primary $\alpha-Al$ structure, whereas the grey fibrous dense constituents are eutectic silicon.

Microstructure formation is highly dependent on the cooling rate. The results in Figure 5(a) indicate that a high cooling rate resulted in the formation of a more compact and finer primary grain structure. In comparison to the other three cooling rate conditions, the highest cooling rate of 1.9 °C/s produced the smallest grain size of 40.96 μm . As for the lowest cooling rate of 0.16 °C/s, the grain size throughout the specimen is inconsistent, and the variation of measurement is comparatively high, which its reading ranging from 79.29 μm and capped at 252.89 μm . The data analysis also reveals that high cooling rates lead to fine and highly oriented dendrites, whereas low cooling rates result in large and coarse dendrites. The increment of cooling rate accelerates the heat extraction from the melt, hence, the solidification time is shortened, causing the nuclei growth to be suppressed [19]. Moreover, this finding is consistent with solidification theory which states that rapid solidification reduces the time required for diffusion, resulting in a more refined dendritic microstructure. A tiny dendritic size implies a fine structure, with all the related benefits, such as finer intermetallic, improved micro-homogeneity, and less porosity [20]. All these desirable characteristics of the cast structure contribute to its superior mechanical properties. Besides that, the shape factor of the primary grain was determined from the average circularity and the average aspect ratio. A circularity with a value of 1.0 indicates a perfect circle. An increasingly elongated shape shall be observed as the value approaches zero. Also, a particle with an aspect ratio of 1:1 is a perfect circle.

Based on the results presented in Figure 5(b), most primary phase grains have circularity ranging from 0.5 to 0.6, except for the sample subjected to slow cooling at the crucible wall whose average grain circularity is below 0.5. In Figure 5(c), it was also found that most of the samples seem to be ellipse- or oval-shaped as their major axis is double their minor axis, where their aspect ratio is 2:1.



Fig. 4. Microstructure evolution of the solidified material at the crucible centre (left) and at the crucible wall (right) with cooling rate of (a), (b) 0.16 °C/s, (c), (d) 1.0 °C/s, (e), (f) 1.3 °C/s, and (g), (h) 1.9 °C/s. (5x magnification)

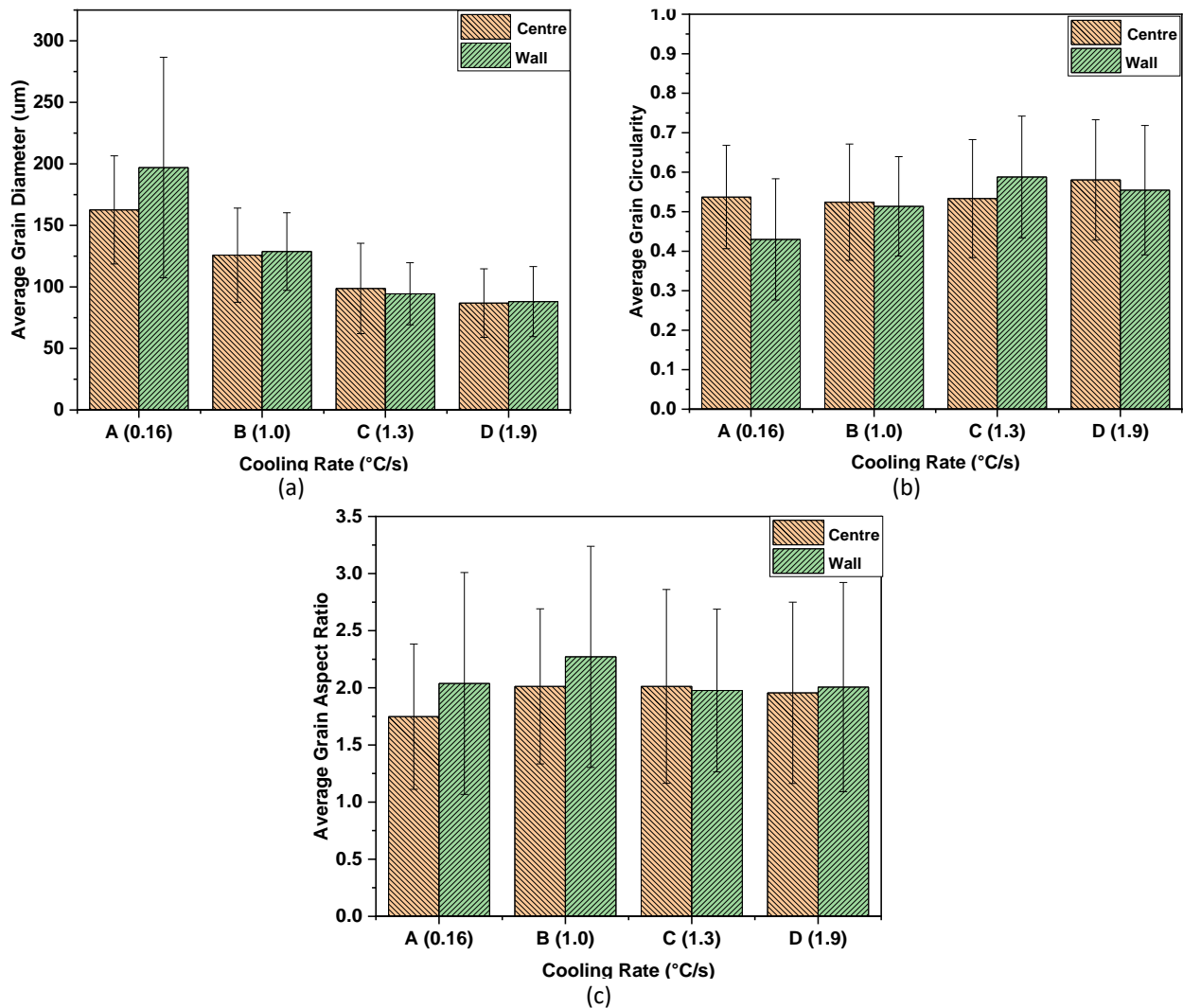


Fig. 5. Grain size measurement of the solidified material at the crucible centre and wall in the aspect of (a) average diameter, (b) average circularity, and (c) average aspect ratio of the primary grain structure

4. Conclusions

In order to determine the optimal process parameters in the semisolid metal processing of the Al-9Si cast alloy, a thermal analysis study of this material was conducted. The results from this study reveal the following

- i. The solidification parameters are weakly correlated to the change of the cooling rate.
- ii. A significant grain refinement with an increase in cooling rate is observed. Increasing the cooling rate of the Al-9Si cast alloy from 0.16 °C/s to 1.9 °C/s reduced the primary dendrite size from 162.61 µm to 86.86 µm. Samples with a higher cooling rate (1.3 °C/s and 1.9 °C/s in particular) have primary grain sizes lower than 100 µm.
- iii. As the cooling rate increases, the solidification period decreases, and the critical phase transformation shifts accordingly in terms of time. The increase in cooling rate facilitates the nucleation rate and the crystal growth is suppressed, hence producing a greater amount of fine primary phase grains.
- iv. The solid fraction of the Al-9Si cast alloy in the semisolid state, at which 0.5 to 0.7 in particular, indicates a negligible change with the cooling rate.

- v. The optimal temperature of the Al-9.7Si cast alloy for the semisolid metal processing is $560 \pm 3^\circ\text{C}$ at $f_s=0.5$, or/and $556 \pm 2^\circ\text{C}$ at $f_s=0.7$.

Acknowledgement

The authors are obliged to the Ministry of Higher Education for providing financial support under Fundamental Research Grant Scheme (FRGS) No. FRGS/1/2019/TK03/UMP/03/4 (University reference RDU1901166) and Universiti Malaysia Pahang for the use of the laboratory facilities.

References

- [1] Browne, D. J., M. J. Hussey, A. J. Carr, and D. Brabazon. "Direct thermal method: new process for development of globular alloy microstructure." *International Journal of Cast Metals Research* 16, no. 4 (2003): 418-426. <https://doi.org/10.1080/13640461.2003.11819618>
- [2] Xiao, Guanfei, Jufu Jiang, Yingze Liu, Ying Wang, and Baoyong Guo. "Recrystallization and microstructure evolution of hot extruded 7075 aluminum alloy during semi-solid isothermal treatment." *Materials Characterization* 156 (2019): 109874. <https://doi.org/10.1016/j.matchar.2019.109874>
- [3] Luo, Xiaoqiang, Yongjun Han, Qingbin Li, Xiaoming Hu, Yanling Li, and Yanbiao Zhou. "Effect of pouring temperature on microstructure and properties of A356 alloy strip by a novel semisolid micro fused-casting for metal." *Journal of Wuhan University of Technology-Materials and Science* 34 (2019): 1205-1209. <https://doi.org/10.1007/s11595-019-2179-7>
- [4] Lozares, Jokin, Gorka Plata, Iñaki Hurtado, Andrea Sánchez, and Iñigo Loizaga. "Near solidus forming (NSF): Semi-solid steel forming at high solid content to obtain as-forged properties." *Metals* 10, no. 2 (2020): 198. <https://doi.org/10.3390/met10020198>
- [5] Omar, M. Z., E. J. Palmiere, A. A. Howe, Helen V. Atkinson, and P. Kapranos. "Thixoforming of a high performance HP9/4/30 steel." *Materials Science and Engineering: A* 395, no. 1-2 (2005): 53-61. <https://doi.org/10.1016/j.msea.2004.12.013>
- [6] Kapranos, Plato. "Current state of semi-solid net-shape die casting." *Metals* 9, no. 12 (2019): 1301. <https://doi.org/10.3390/met9121301>
- [7] Rosso, Mario. "Thixocasting and rheocasting technologies, improvements going on." *Journal on Achievements in Materials and Manufacturing Engineering* 54, no. 1 (2012): 110-119.
- [8] Omar, Mohd Z., Helen V. Atkinson, Eric J. Palmiere, Andrew A. Howe, and Plato Kapranos. "Microstructural development of HP9/4/30 steel during partial remelting." *Steel Research International* 75, no. 8-9 (2004): 552-560. <https://doi.org/10.1002/srin.200405810>
- [9] Dahle, A. K., and D. H. StJohn. "Rheological behaviour of the mushy zone and its effect on the formation of casting defects during solidification." *Acta Materialia* 47, no. 1 (1998): 31-41. [https://doi.org/10.1016/S1359-6454\(98\)00342-5](https://doi.org/10.1016/S1359-6454(98)00342-5)
- [10] Salleh, M. S., M. Z. Omar, J. Syarif, and M. N. Mohammed. "An overview of semisolid processing of aluminium alloys." *International Scholarly Research Notices* 2013, no. 1 (2013): 679820. <https://doi.org/10.1155/2013/679820>
- [11] Kirkwood, David H., Michel Suéry, Plato Kapranos, Helen V. Atkinson, and Kenneth P. Young. *Semi-solid processing of alloys*. Vol. 124. Berlin: Springer, 2010. <https://doi.org/10.1007/978-3-642-00706-4>
- [12] Camacho, A. Maciel, H. V. Atkinson, P. Kapranos, and B. B. Argent. "Thermodynamic predictions of wrought alloy compositions amenable to semi-solid processing." *Acta Materialia* 51, no. 8 (2003): 2319-2330. [https://doi.org/10.1016/S1359-6454\(03\)00040-5](https://doi.org/10.1016/S1359-6454(03)00040-5)
- [13] Abd Razak, Nur Azhani, Asnul Hadi Ahmad, Mohd Maarof Rashidi, and Sumsun Naher. "An investigation of semisolid Al7075 feedstock billet produced by a gas-assisted direct thermal method." *The International Journal of Advanced Manufacturing Technology* 114 (2021): 1233-1240. <https://doi.org/10.1007/s00170-021-06924-8>
- [14] Bäckerud, Lennart, Guocai Chai, and Jarmo Tamminen. *Solidification characteristics of aluminum alloys*. American Foundrymen's Society, 1990.
- [15] Chávez-Zamarripa, Rubén, J. Angelica Ramos-Salas, José Talamantes-Silva, Salvador Valtierra, and Rafael Colás. "Determination of the dendrite coherency point during solidification by means of thermal diffusivity analysis." *Metallurgical and Materials Transactions A* 38 (2007): 1875-1879. <https://doi.org/10.1007/s11661-007-9212-8>
- [16] Shin, Je-Sik, and Zin-Hyoung Lee. "Computer-aided cooling curve analysis of A356 aluminum alloy." *Metals and Materials International* 10 (2004): 89-96. <https://doi.org/10.1007/BF03027368>
- [17] Veldman, Natalia LM, Arne K. Dahle, David H. StJohn, and Lars Arnberg. "Dendrite coherency of Al-Si-Cu alloys." *Metallurgical and Materials Transactions A* 32 (2001): 147-155. <https://doi.org/10.1007/s11661-001-0110-1>

- [18] Xu, Kai, Jianjun Wang, and Shuquan Zhang. "Effect of heat treatment on the microstructure and properties of in-situ Mg₂Si reinforced hypereutectic Al-18% Si matrix composites." *Materials Research Express* 7, no. 8 (2020): 086515. <https://doi.org/10.1088/2053-1591/abaea2>
- [19] Razak, N. A., A. H. Ahmad, and M. R. Maarof. "Thermal profile and microstructure of wrought aluminium 7075 for semisolid metal processing." *International Journal of Automotive and Mechanical Engineering* 17, no. 2 (2020): 7842-7850. <https://doi.org/10.15282/ijame.17.2.2020.03.0584>
- [20] Snopiński, Przemysław, Mariusz Król, Tomasz Tański, and Beata Krupińska. "Effect of cooling rate on microstructural development in alloy ALMG9." *Journal of Thermal Analysis and Calorimetry* 133 (2018): 379-390. <https://doi.org/10.1007/s10973-018-7313-9>